Research Article

SnO₂/Graphene Composite with High Lithium Storage Capability for Lithium Rechargeable Batteries

Haegyeom Kim[1], Sung-Wook Kim[2], Young-Uk Park[2], Hyeokjo Gwon[2], Dong-Hwa Seo[2], Yuhee Kim[4], and Kisuk Kang[1, 2, 3] (✉)

[1] Graduate School of Energy, Environment, Water, and Sustainability, Korea Advanced Institute of Science and Technology (KAIST), 335 Gwahangno, Yuseong-gu, Daejeon 305-701, Republic of Korea

[2] Department of Materials Science and Engineering, KAIST, 335 Gwahangno, Yuseong-gu, Daejeon 305-701, Republic of Korea

[3] KAIST Institute for Eco-energy, Nanocentury, KAIST, 335 Gwahangno, Yuseong-gu, Daejeon 305-701, Republic of Korea

[4] Korea Institute of Science and Technology (KIST), 39-1 Hawolgok-dong, Wolsong-gil 5, Seongbuk-gu, Seoul 136-791, Republic of Korea

ABSTRACT

SnO₂/graphene nanocomposites have been fabricated by a simple chemical method. In the fabrication process, the control of surface charge causes echinoid-like SnO₂ nanoparticles to be formed and uniformly decorated on the graphene. The electrostatic attraction between a graphene nanosheet (GNS) and the echinoid-like SnO₂ particles under controlled pH creates a unique nanostructure in which extremely small SnO₂ particles are uniformly dispersed on the GNS. The SnO₂/graphene nanocomposite has been shown to perform as a high capacity anode with good cycling behavior in lithium rechargeable batteries. The anode retained a reversible capacity of 634 mA·h·g⁻¹ with a coulombic efficiency of 98% after 50 cycles. The high reversibility can be attributed to the mechanical buffering by the GNS against the large volume change of SnO₂ during delithiation/lithiation reactions. Furthermore, the power capability is significantly enhanced due to the nanostructure, which enables facile electron transport through the GNS and fast delithiation/lithiation reactions within the echinoid-like nano-SnO₂. The route suggested here for the fabrication of SnO₂/graphene hybrid materials is a simple economical route for the preparation of other graphene-based hybrid materials which can be employed in many different fields.

KEYWORDS

1. Introduction

There is an intensive research effort aimed at developing new electrode materials for lithium rechargeable batteries [1–3]. While graphite, which is used as an anode material in current lithium rechargeable batteries, has served as a reliable electrode due to its low operating voltage and good cyclability, its low specific capacity of about 372 mA·h·g⁻¹ hinders the adoption of lithium batteries in new applications such as electric vehicles and large scale energy storage units, which demand higher levels of energy and power density. Therefore, many researchers have focused on exploring new anode materials with higher energy and power density than existing electrodes [4–8]. Of these, elements such as Si and Sn that alloy

Address correspondence to matlgen1@kaist.ac.kr

with Li are attractive candidates for replacing graphite due to their exceptionally high theoretical capacities [9–12]. Because these materials can typically store more than one lithium ion per one metal atom through the alloying reaction [1, 13], they are capable of delivering high energy. For example, the theoretical capacity is about 4200 $mA\cdot h\cdot g^{-1}$ for Si and about 994 $mA\cdot h\cdot g^{-1}$ for Sn [9, 11]. However, these alloying reactions are often associated with a large volume change during the charge/discharge processes, and therefore, show a rapid fading of capacity during cycling [9].

Several approaches have been suggested to deal with the problem of the large volume change. One approach involves the fabrication of an electrode based on nanostructures such as nanoparticles, nanowires, nanotubes or porous nanostructures [6, 14, 15]. Another approach involves the doping of an inactive element to reduce the volume change. A third approach involves making a nanocomposite with an inactive matrix and active components [16–18]. In the nanocomposite, the inactive matrix serves as a mechanical buffer for the large volume change of the active materials; as a result, the composite exhibits better cycling behavior than the active materials alone [18]. Some compounds transform to a nanocomposite material during the initial battery cycle. For instance, SnO_2 forms an Li_2O matrix with metallic nano-Sn dispersed within it during the first discharge. On further lithiation, the Sn metal nanoparticles alloy with Li to form $SnLi_x$ as the active component. The inactive Li_2O matrix helps to buffer the volume change of the $SnLi_x$ alloy and prevents Sn nanoparticles from being mechanically pulverized or disconnected in repeated charge/discharge processes [19–22]. However, the electrically insulating characteristics of the Li_2O matrix formed in the first discharge can cause a problem of poor electronic conductivity in the electrode [10, 23], and this problem can cause a severe deterioration in the rate capability of the electrode and gives a low efficiency in energy storage due to the large polarization [24].

Here, we demonstrate that the incorporation of graphene with its large surface area, superior electronic conductivity, and mechanical flexibility can significantly improve the electrochemical activity of SnO_2 [25, 26]. A composite with SnO_2 nanoparticles uniformly dispersed on the graphene is expected to have three main benefits. Firstly, the high surface area of graphene can effectively provide a percolating network throughout the electrode, ensuring facile electron transport. Secondly, the high mechanical flexibility of graphene helps to accommodate the volume change induced by $SnLi_x$ and the Li_2O matrix. And, finally, the close contact between the SnO_2 nanoparticles and the graphene can minimize the electrical isolation of nanoparticles during battery cycles. In this study, we introduce a simple and new synthetic route for fabricating an SnO_2/graphene composite of nanoscale echinoid-like SnO_2 particles and graphene. The uniform dispersion of SnO_2 on the graphene surface is ensured by controlling the zeta potential of each component. The diverse functional groups of chemically reduced graphene make it easy for the surface of graphene nanosheets (GNSs) to become negatively charged [27]. Because the SnO_2 particles can have a positive surface charge in a specific pH range, the SnO_2 particles can electrostatically attach themselves on the GNS. The resulting nanocomposite is demonstrated to be an excellent anode material with high energy and power, and good cyclability.

2. Methods

The hybrid SnO_2/graphene composite was fabricated in three steps. The first step involved the production of graphite oxide from graphite powder. The graphite oxide was synthesized by means of a modified Hummers' method [28]. 1 g of graphite, 1 g of $NaNO_3$, and 46 mL of concentrated H_2SO_4 were stirred together in an ice bath for 30 min, followed by the slow addition of 5 g of $KMnO_4$. The mixture was stirred for 2 h at 35 °C. 100 mL of de-ionized (DI) water was slowly added to this mixture and stirred for 15 min after which 8 mL of H_2O_2 (30%) was added. The solution was filtered and washed with 150 mL of HCl (10%) and 100 mL of DI water [29]. The resulting solution was subjected to centrifugation (4000 r/min, 5 min) to retrieve the graphite oxide. In the second step, 0.1 g of the retrieved graphite oxide was added to 400 mL of DI water. The mixture was sonicated for 90 min. Graphene oxide (GO) layers were exfoliated from the graphite oxide through this sonication process. In the last step,

50 mg of Sn metal powder (150 nm) and 400 mL of DI water were added to the GO solution. 3800 μL of NH₄OH and 250 μL of hydrazine (NH₂NH₂, 35 wt.%) were also added to reduce GO [30, 31]. During this last step, tin particles were etched and oxidized to tin oxide (SnO₂). The solution was stirred for 8 h at 80 ℃ and then filtered. The pH of the solution was controlled in the range of 4 to 5 by means of addition of HCl to ensure the uniform dispersion of SnO₂ particles on the GNS. Figure 1 shows a schematic illustration of the process of fabrication of the SnO₂/graphene nanocomposite.

In order to improve the crystallinity of the SnO₂ and remove the residual water molecules and functional groups from the GNS, the product was heated at 500 ℃ for 4 h under an argon atmosphere.

The structure of the product was characterized by X-ray diffraction (XRD) using a Rigaku D/MAX-RC (12 kW) diffractometer with Cu Kα radiation (λ = 1.518 Å), with a scan range of 20–60°. The SnO₂/graphene composite was analyzed with the aid of a high resolution dispersive Raman microscope (HORIBA Jobin Yvon LabRAM HR UV/Vis/NIR) with Raman shifts measured from 1200 cm⁻¹ to 1800 cm⁻¹. The morphology of the composite was analyzed with a scanning electron microscope (SEM, Philips XL-30S-FEG) and a transmission electron microscope (TEM, JEOL JEM 2100F). The amount of carbon in the composite was determined by elemental analysis (Fisons EA 1110 elemental analyzer).

The electrodes were prepared without further addition of conductive carbon sources by simply mixing the SnO₂/graphene nanocomposite (90 wt.%) with polyvinylidene fluoride (10 wt.%) in *N*-methyl-2-pyrrolidone as a solvent for an electrochemical characterization. The resultant slurry was uniformly pasted on Cu foil. The electrodes were dried at 120 ℃ for 2 h and then roll-pressed. In a glove box, the test cells were assembled into two-electrode cells with an Li metal counter electrode, a separator (Celgard 2400), and an electrolyte of 1 mol/L lithium hexafluorophosphate in a 1:1 mixture of ethylene carbonate and dimethyl carbonate (Techno Semichem). A multichannel potentiogalvanostat (WonATech, WBCS3000) was used to obtain electrochemical profiles in the voltage range 0.001 V to 3.0 V at various current densities.

For comparison, a bare graphene electrode and a commercial SnO₂ (approximately 100 nm) electrode mixed with graphite (6:4) were prepared under the same conditions.

3. Results and discussion

The fabrication process of the SnO₂/graphene nanocomposite is schematically illustrated in Fig. 1. The GO was obtained from graphite by using strong oxidation agents. The subsequent GO reduction process involved the addition of Sn metal (approximately 150 nm). During the GO reduction process, the added Sn metal was etched and oxidized to SnO₂. Initially, the pH of the mixture was not controlled.
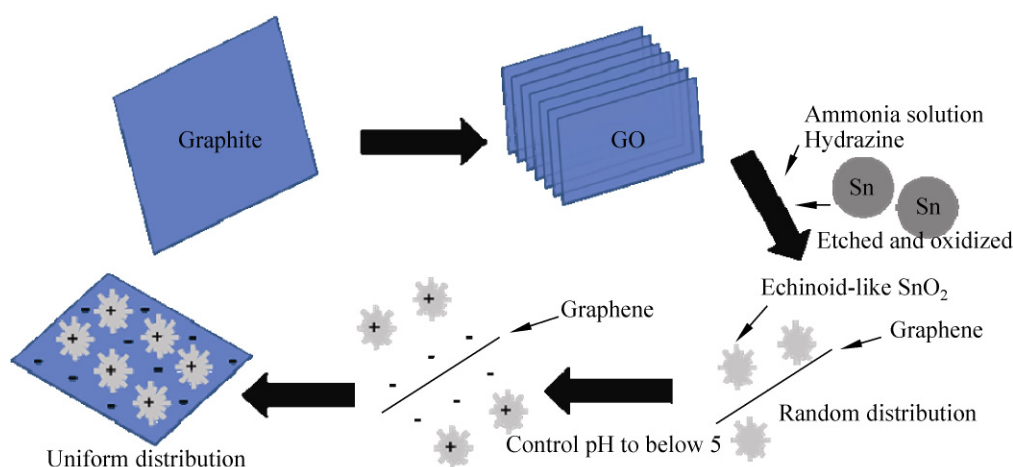
Figure 1   Schematic illustration of the fabrication of the SnO₂/graphene composite

The resulting nanocomposite was analyzed by XRD, (Fig. 2(a)). The major diffraction peaks can be indexed to those of SnO_2 (JCPDS card No. 41-1445). Furthermore, the characteristic diffraction peak of the GNS confirms the presence of graphene in the composite. There are no observable impurity peaks, not even those of Sn or SnO. A calculation using the Scherrer equation gives a particle size of 4.5 nm (as shown in the inset of Fig. 2(a)) [32, 33].

TEM analysis of the composite (Fig. 2(b)) shows that the primary particle size of the SnO_2 was about 4 nm, which is consistent with the average crystallite size calculated from the XRD pattern. We found that these small primary particles were aggregated into large echinoid-like secondary particles (of about 14 nm in size). The spacing between the lattice fringes in the high resolution TEM image was about 0.35 nm (as shown in the inset of Fig. 2(b), which agrees with the (110) spacing of SnO_2). In addition, the crystalline structure of the SnO_2 was confirmed by means of selected area electron diffraction (Fig. 2(c)). The ring patterns and the corresponding lattice spacings are consistent with the XRD analysis.
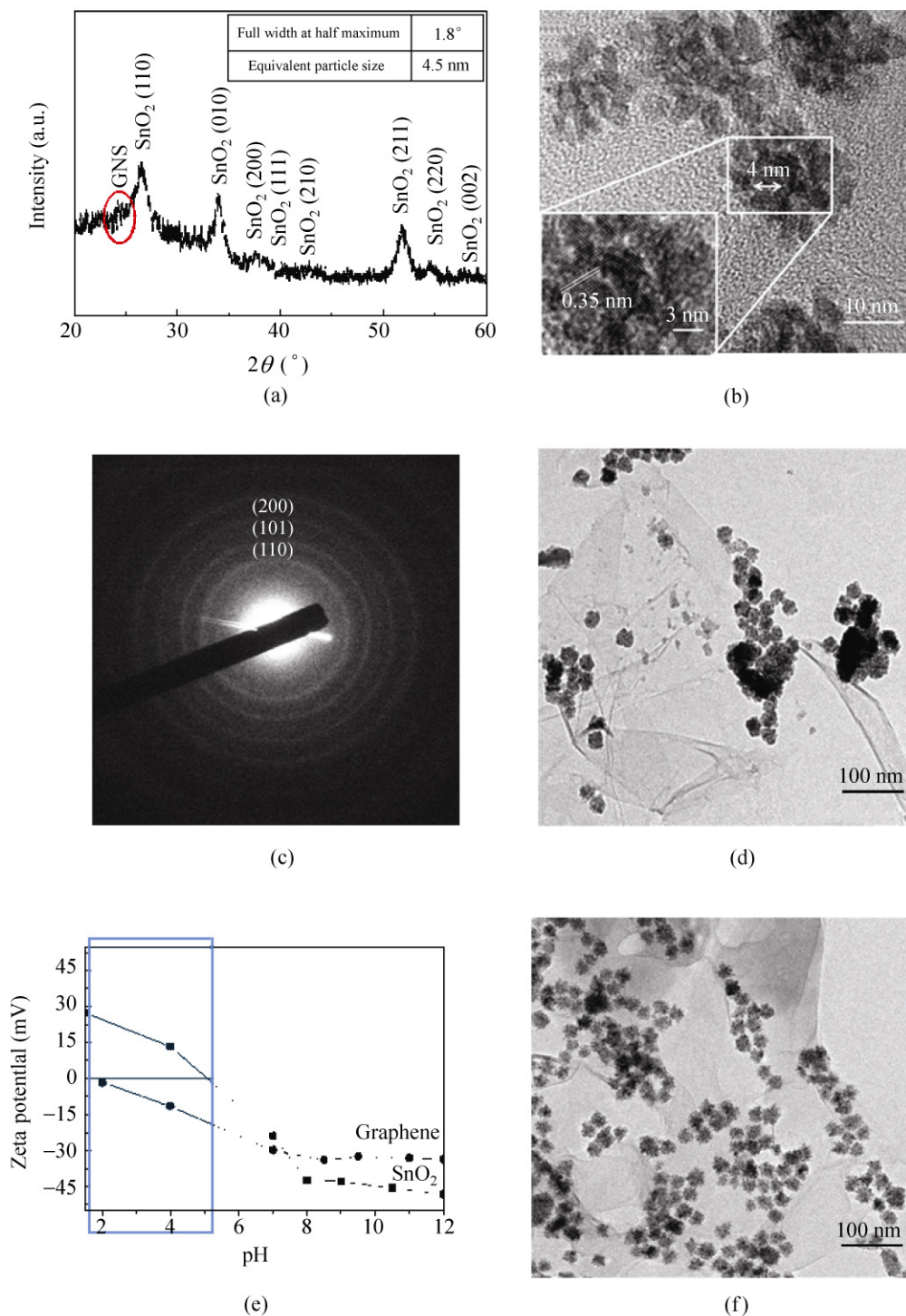
The morphology of the SnO_2/graphene composite was further analyzed by low magnification TEM (Fig. 2(d)). Although small echinoid-like particles can be easily observed on the GNS, there were many regions where these particles are severely agglomerated or even separated from the GNS. To ensure a uniform dispersion of the SnO_2 nanoparticles on the graphene, we investigated the surface charges of the SnO_2 and graphene as a function of pH. Figure 2(e) shows the measured zeta potentials of the graphene and SnO_2 with varying pH. The zeta potential results indicate that the graphene and SnO_2 are both negatively charged under our initial experimental reduction conditions, involving a typical pH of about 7 (as illustrated by the dotted line in Fig. 2(e)). This suggests that a more uniform mixture of SnO_2 on the graphene can be achieved if we ensure that the SnO_2 and graphene have opposite surface charges. The plot of zeta potential against pH indicates that SnO_2 has a positive charge and graphene has a negative charge in a pH range of 2 to 5 (the shaded region in Fig. 2(e)). Accordingly, we added HCl to keep the pH of the solution between

4 and 5. Figure 2(f) shows the morphology of the SnO_2/graphene composite prepared with control of pH which confirms that the SnO_2 nanoparticles are more uniformly dispersed on the graphene without any severe aggregation.
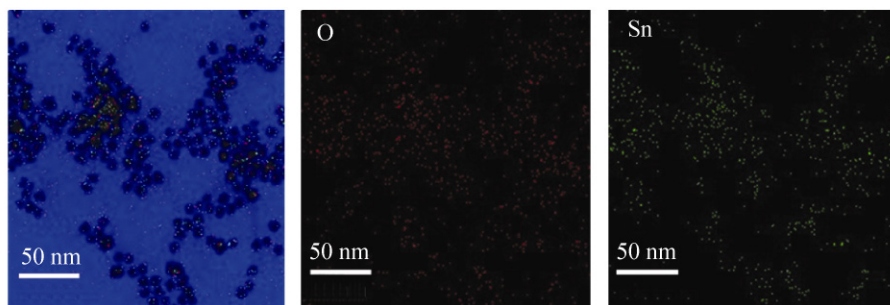
The composition mapping of the TEM image of the composite indicates that the echinoid-like particles are composed of tin and oxygen (Fig. 3). The oxidation of Sn to SnO_2 during the reduction process is attributed mainly to the presence of an ammonia solution. Figures S-1 and S-2 in the Electronic Supplementary Material (ESM) illustrate the results of oxidation of Sn in different environments: firstly, in a mixture of hydrazine and ammonia solution; secondly, in an ammonia solution alone; thirdly, in a solution of hydrazine alone. Significant oxidation of Sn occurs only when the ammonia solution is added. Furthermore, in the absence of graphene, a small amount of Sn metal was detected after the reaction. This implies that the functional groups of graphene also, to some extent, contribute to the oxidation of Sn metal during the reduction process.

SEM images of the SnO_2/graphene composite (Fig. 4) show that the SnO_2 particles are uniformly distributed on a wrinkled GNS. The energy dispersive spectrum of this region confirms the presence of Sn and O (as shown in the inset of Fig. 4(a)). Figure 4(b) shows a cross-sectional SEM image of the composite. The SnO_2 particles are well inserted between the entangled graphene layers. The graphene layers in the composite were investigated by means of Raman spectroscopy (Fig. 5). The broad peaks at 1355 cm^{-1} and 1605 cm^{-1}, which are assigned to the D and G peaks of the graphene, respectively, confirm the presence of the graphene in the composite [34–36]. Elemental analysis revealed that the content by mass of carbon, mostly graphene, was about 38%. Therefore the complete electrode used for electrochemical tests consists of 56 wt.% of SnO_2, 34 wt.% of graphene and 10 wt.% of binder.

The electrochemical properties of the SnO_2/graphene composite were measured by means of galvanostatic charge/discharge cycling at a current density of 0.1 $A \cdot g^{-1}$ in the voltage range 0.001 V to 3.0 V. The specific capacities given below are based on the

Figure 2 XRD pattern and TEM images of the SnO$_2$/graphene composite: (a) XRD pattern of the SnO$_2$/graphene composite (the inset gives the full width at half-maximum of the (211) reflection and the particle size calculated from the Scherrer equation); (b) high magnification TEM image of the SnO$_2$/graphene composite in which small SnO$_2$ primary particles (~4 nm) form larger secondary particles as large as 14 nm; (c) the selected area electron diffraction pattern of the SnO$_2$/graphene composite; (d) TEM image of the SnO$_2$/graphene composite prepared without pH control; (e) zeta-potentials of graphene and SnO$_2$ as a function of pH; (f) the SnO$_2$/graphene composite prepared with control of pH

Figure 3   Energy dispersive spectroscopic mapping of the SnO$_2$/graphene composite which reveals that the echinoid-like particles are composed of Sn and O
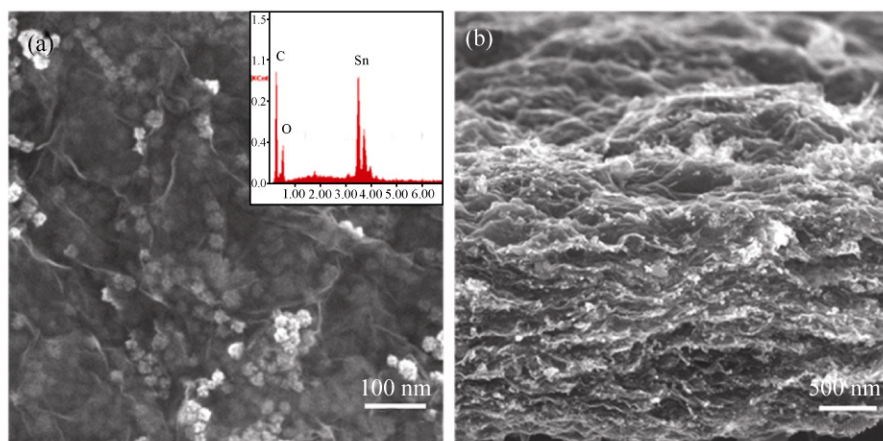
**Figure 4**   (a) SEM image of the SnO$_2$/graphene in which SnO$_2$ particles are uniformly distributed on the graphene with the energy dispersive spectrum in the inset; (b) cross-sectional SEM image of the composite
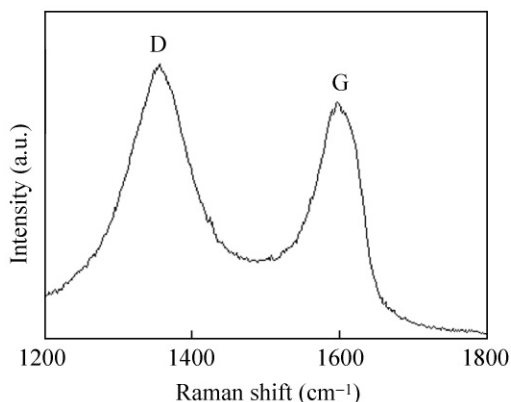
Figure 5   Raman spectrum of the SnO$_2$/graphene composite

mass of the composite. Figure 6(a) shows the typical charge/discharge profiles of the composite in the 2nd, 5th, and 10th cycles. The shape of the profiles did not change significantly during cycling, which shows the stability of the composite as an anode. The first discharge capacity was 1719 mA·h·g^{-1}, and the reversible charge capacity was about 852 mA·h·g^{-1}. The irreversible

capacity may be caused by the formation of a solid electrolyte interphase or Li-ion reaction with unreduced functional groups on the GNS. However, after the first cycle, the SnO$_2$/graphene anode showed highly reversible behavior. The anode retained a reversible capacity of 634 mA·h·g^{-1} with a coulombic efficiency of 98% after 50 cycles (Fig. 6(b)). As shown in Fig. 6(c), the reversibility of the SnO$_2$/graphene anode is higher than that of anodes prepared from either bare graphene or SnO$_2$ mixed with conductive graphite. Furthermroe, the bare graphene and SnO$_2$ anodes rapidly lost their capacity, whereas the hybrid SnO$_2$/graphene delivered a high capacity over an extended number of cycles. The high reversible capacity was well retained even at elevated current densities. Figure 6(d) shows the power capability of the electrode at various rates. The reversible capacity of the SnO$_2$/graphene composite at 2 A·g^{-1} was 389 mA·h·g^{-1}, which is even higher than the theoretical capacity of a conventional commercial graphite anode (372 mA·h·g^{-1}).
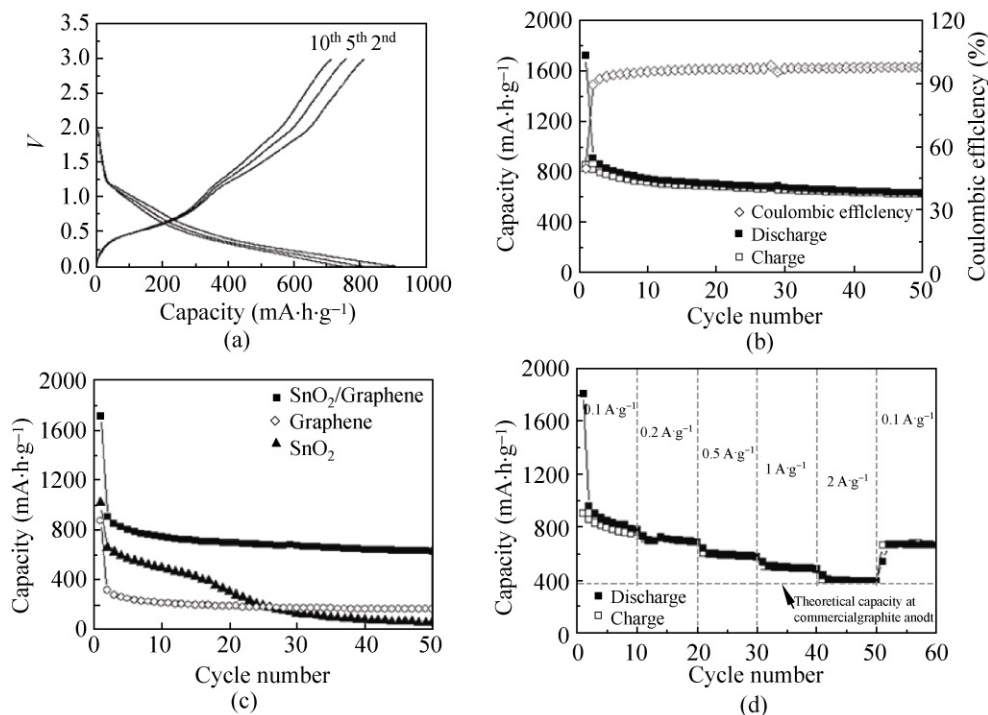
Figure 6　Galvanostatic analysis of the SnO_2/graphene composite: (a) charge/discharge profiles; (b) cyclability of the SnO_2/graphene composite with a current density of 0.1 A·g^{-1}; (c) cyclability of the SnO_2/graphene, SnO_2–graphite composite, and bare graphene; (d) rate capability of the SnO_2/graphene

The high reversibility and power capability of the SnO_2/graphene composite can be attributed to the unique structure of the composite, in which extremely small echinoid-like SnO_2 particles are uniformly dispersed on an electrically conductive GNS. In the composite, the Li_2O matrix which is formed during the initial discharge, and the GNS which has excellent mechanical flexibility can both work as mechanical buffers to mitigate the huge volume change of the $SnLi_x$ alloy during the charge/discharge processes [25, 26]. Furthermore, the use of extremely small echinoid-like SnO_2 nanoparticles can help reduce the intrinsically large volume change [37]. The problem of poor electronic conductivity and low rate capability associated with the insulating Li_2O can also be mitigated by the use of an electrically conductive GNS network and extremely small SnO_2 nanoparticles. Because of the nanoscale SnO_2, the insulating layer of the Li_2O matrix is extremely thin, and therefore, electron transport through the insulating Li_2O matrix is higher than for thicker layers. The GNS network

has good electrical conductivity, and furthermore, the three-dimensional nature of the network provides a useful mechanical and electronic framework for the dispersion of nanoparticles in the electrode. Because the GNS makes a network throughout the electrode, the contact loss of the entire electrode is significantly reduced. Therefore, the electron transfer during the charge/discharge processes is greatly improved by the percolating electronic path of the GNS network [38, 39]. However, there is a possibility that the nano-sized particles become aggregated after a prolonged number of battery cycles resulting in a slight capacity decay. We are currently investigating ways to overcome this problem.

This study clearly demonstrates that an intelligent nanostructure can drastically enhance the electro-chemical performance of an electrode, especially one involving alloying reactions which generally suffer from a huge volume change and low electronic conductivity. Nanostructures that use a graphene framework should also be capable of being more

widely applied to other promising alloying reaction electrodes in order to enhance their electrochemical activities.

4. Summary

We have demonstrated a simple and straightforward fabrication route for a SnO_2/graphene hybrid composite. Under a controlled surface charge, echinoid-like nano SnO_2 was produced and formed a composite in which SnO_2 particles are uniformly dispersed on the GNS. The resulting SnO_2/graphene electrode exhibits a high reversible capacity that reaches levels as high as 634 mA·h·g^{-1} at the 50th cycle. A high rate capability was also achieved. The composite can deliver 389 mA·h·g^{-1} at a rate of 2 A·g^{-1}. This promising electrochemical performance was achieved as a result of the unique nanostructure of the composite, which means that the GNS works as a mechanical buffer and a conductive network as well as an active electrode material. Our hybrid assembly principle can be further utilized to create a variety of functional hybrid nanomaterials.

Acknowledgements

Electronic Supplementary Material: XRD patterns and SEM images that confirm the etching and oxidation behavior of Sn in the aid of ammonia is available in the online version of this article at http://dx.doi.org/10.1007/s12274-010-0050-4 and is accessible free of charge.

References

[1] Tarascon, J. M.; Armand, M. Issues and challenges facing rechargeable lithium batteries. *Nature* **2001**, *414*, 359–367.

[2] Lee, Y. J.; Yi, H.; Kim, W. J.; Kang, K.; Yun, D. S.; Strano, M. S.; Ceder, G.; Belcher, A. M. Fabricating genetically engineered high-power lithium-ion batteries using multiple virus genes. *Science* **2009**, *324*, 1051–1055.

[3] Ryu, J.; Kim, S. W.; Kang, K.; Park, C. B. Synthesis of diphenylalanine/cobalt oxide hybrid nanowires and their application to energy storage. *ACS Nano* **2010**, *4*, 159–164.

[4] Zhang, W. M.; Hu, J. S.; Guo, Y. G.; Zheng, S. F.; Zhong, L. S.; Song, W. G.; Wan, L. J. Tin-nanoparticles encapsulated in elastic hollow carbon spheres for high-performance anode material in lithium-ion batteries. *Adv. Mater.* **2008**, *20*, 1160–1165.

[5] Lou, X. W.; Wang, Y.; Yuan, C.; Lee, J. Y.; Archer, L. A. Template-free synthesis of SnO_2 hollow nanostructure with high lithium storage capacity. *Adv. Mater.* **2006**, *18*, 2325–2329.

[6] Yao, J.; Shen, X.; Wang, B.; Liu, H.; Wang, G. *In situ* chemical synthesis of SnO_2–graphene nanocomposite as anode materials for lithium-ion batteries. *Electrochem. Commun.* **2009**, *11*, 1849–1852.

[7] Liu, Y.; Zhang, X. Effect of calcination temperature on the morphology and electrochemical properties of Co_3O_4 for lithium-ion battery. *Electrochim. Acta* **2009**, *54*, 4180–4185.

[8] Paek, S. M.; Yoo, E.; Honma, I. Enhanced cyclic performance and lithium storage capacity of SnO_2/graphene nanoporous electrodes with three-dimensionally delaminated flexible structure. *Nano Lett.* **2009**, *9*, 72–75.

[9] Chan, C. K.; Peng, C. K.; Liu, G.; McIlwrath, K.; Zhang, X. F.; Huggins, R. A.; Cui, Y. High-performance lithium battery anodes using silicon nanowires. *Nat. Nanotechnol.* **2008**, *3*, 31–35.

[10] Chou, S. L.; Wang, J. Z.; Choucair, M.; Liu, H. K.; Stride, J. A.; Dou, S. X. Enhanced reversible lithium storage in a nanosize silicon/graphene composite. *Electrochem. Commun.* **2010**, *12*, 303–306.

[11] Wang, G.; Wang, B.; Wang, X.; Park, J.; Dou, S.; Ahn, H.; Kim, K. Sn/graphene nanocomposite with 3D architecture for enhanced reversible lithium storage in lithium ion batteries. *J. Mater. Chem.* **2009**, *19*, 8378–8384.

[12] Beaulieu, L. Y.; Hewitt, K. C.; Turner, R. L.; Bonakdarpour, A.; Abdo, A. A.; Christensen, L.; Eberman, K. W.; Krause, L. J.; Dahn, J. R. The electrochemical reaction of Li with amorphous Si–Sn alloys. *J. Electrochem. Soc.* **2003**, *150*, A149–A156.

[13] Poizot, P.; Laruelle, S.; Grugeon, S.; Dupont, L.; Tarascon,

J. M. Nano-sized transition-metal oxides as negative-electrode materials for lithium-ion batteries. *Nature* **2000**, *407*, 496–499.

[14] Zhao, N. H.; Yang, L. C.; Zhang, P.; Wnag, G. J.; Wang, B.; Yao, B. D.; Wu, Y. P. Polycrystalline SnO_2 nanowires coated with amorphous carbon nanotubes as anode material for lithium ion batteries. *Mater. Lett.* **2010**, *64*, 972–975.

[15] Wen, Z.; Wang, Z.; Zhang, Z.; Li, J. *In situ* growth of mesoporous SnO_2 on multiwalled carbon nanotubes: A novel composite with porous-tube structure as anode for lithium batteries. *Adv. Funct. Mater.* **2007**, *17*, 2772–2778.

[16] Hassoun, J.; Derien, G.; Panero, S.; Scrosati, B. The role of the morphology in the response of Sb–C nanocomposite electrodes in lithium cells. *J. Power Sources* **2008**, *183*, 339–343.

[17] Park, C. M.; Sohn, H. J. Quasi-intercalation and facile amorphization in layered ZnSb for Li-ion batteries. *Adv. Mater.* **2010**, *22*, 47–52.

[18] Winter, M.; Besenhard, J. O. Electrochemical lithiation of tin and tin-based intermetallics and composites. *Electrochim. Acta* **1999**, *45*, 31–50.

[19] Courteny, I. A.; Dahn, J. R. Electrochemical and *in situ* diffraction studies of the reaction of lithium with tin oxide composites. *J. Electrochem. Soc.* **1997**, *144*, 2045–2052.

[20] Zhang, R.; Lee, J. Y.; Liu, Z. L. Pechini process-derived tin oxide and tin oxide–graphite composites for lithium-ion batteries. *J. Power Sources* **2002**, *112*, 596–605.

[21] Courtney, I. A.; Dahn, J. R. Key factors controlling the reversibility of the reaction of lithium with SnO_2 and Sn_2BPO_6 glass. *J. Electrochem. Soc.* **1997**, *144*, 2943–2948.

[22] Hightower, A.; Delcroix, P.; Caer, G. L.; Huang, C. K.; Ratnakumar, B. V.; Ahn, C. C.; Fultz, B. J. A ^{119}Sn Mossbauer spectrometry study of Li–SnO anode materials for Li-ion cells. *J. Electrochem. Soc.* **2000**, *147*, 1–8.

[23] Aurbach, D.; Nimberger, A.; Markovsky, B.; Levi, E. E.; Sominski, E.; Gedanken, A. Nanoparticles of SnO produced by sonochemistry as anode materials for rechargeable lithium batteries. *Chem. Mater.* **2002**, *14*, 4155–4163.

[24] Guo, Y. G.; Hu, J. S.; Wan, L. J. Nanostructured materials for electrochemical energy conversion and storage devices. *Adv. Mater.* **2008**, *20*, 2878–2887.

[25] Allen, M. J.; Tung, V. C.; Kaner, R. B. Honeycomb carbon: A review of graphene. *Chem. Rev.* **2010**, *110*, 132–145.

[26] Park, S.; Ruoff, R. S. Chemical methods for the production of graphene. *Nat. Nanotechnol.* **2009**, *4*, 217–224.

[27] Han, T. H.; Lee, W. J.; Lee, D. H.; Kim, J. E.; Choi, E. Y.; Kim, S. O. Peptide/graphene hybrid assembly into core/shell nanowires. *Adv. Mater.* **2010**, *22*, 2060–2064.

[28] Hummers, W. S.; Offeman, R. E. Preparation of graphitic oxide. *J. Am. Chem. Soc.* **1958**, *80*, 1339.

[29] Guo, P.; Song, H.; Chen, X. Electrochemical performance of graphene nanosheets as anode material for lithium-ion batteries. *Electrochem. Commun.* **2009**, *11*, 1320–1324.

[30] Stankovich, S.; Piner, R. D.; Chen, X.; Wu, N.; Nguyen, S. T.; Ruoff, R. S. Stable aqueous dispersions of graphitic nanoplatelets via the reduction of exfoliated graphite oxide in the presence of poly(sodium 4-styrenesulfonate). *J. Mater. Chem.* **2006**, *16*, 155–158.

[31] Gómez-Navarro, C.; Weitz, R. T.; Bittner, A. M.; Scolari, M.; Mews, A.; Burghard, M.; Kern, K. Electronic transport properties of individual chemically reduced graphene oxide sheets. *Nano Lett.* **2007**, *7*, 3499–3503.

[32] Cullity, B. D.; Stock, S. R. *Elements of X-ray Diffraction*; 3rd ed.; Prentice Hall: Upper Saddle River, NJ, 2001; pp. 167–171.

[33] Kim, S. W.; Han, T. H.; Kim, J.; Gwon, H.; Moon, H. S.; Kang, S. W.; Kim, S. O.; Kang, K. Fabrication and electro-chemical characterization of TiO_2 three-dimensional nanonet-work based on peptide assembly. *ACS Nano* **2009**, *3*, 1085–1090.

[34] Stankovich, S.; Dikin, D. A.; Piner, R. D.; Kohlhaas, K. A.; Kleinhammes, A.; Jia, Y.; Wu, Y.; Nguyen, S. T.; Ruoff, R. S. Synthesis of graphene-based nanosheets via chemical reduction of exfoliated graphite oxide. *Carbon* **2007**, *45*, 1558–1565.

[35] Tuinstra, F.; Koenig, J. L. Raman spectrum of graphite. *J. Chem. Phys.* **1970**, *53*, 1126–1130.

[36] Ferrari, A. C.; Robertson, J. Interpretation of Raman spectra of disordered and amorphous carbon. *Phys. Rev. B* **2000**, *61*, 14095–14107.

[37] Balan, L.; Ghanbaja, J.; Willmann, P.; Billaud, D. Novel tin–graphite composites as negative electrodes of Li-ion batteries. *Carbon* **2005**, *43*, 2311–3216.

[38] Lee, J. K.; Smith, K. B.; Hayner, C. M.; Kung, H. H. Silicon nanoparticles–graphene paper composites for Li ion battery anodes. *Chem. Commun.* **2010**, *46*, 2025–2027.

[39] Stankovich, S.; Dikin, D. A.; Dommett, G. H. B.; Kohlhaas, K. M.; Zimney, E. J.; Stach, E. A.; Piner, R. D.; Nguyen, S. T.; Ruoff, R. S. Graphene-based composite materials. *Nature* **2006**, *442*, 282–286.